Journal of Molecular Diagnostics, Vol. 5, No. 3, August 2003

Automated Acquisition of Stained Tissue Microarrays for High-Throughput Evaluation of Molecular Targets

Hans Vrolijk,* Willem Sloos,* Wilma Mesker,* Patrick Franken,† Riccardo Fodde,† Hans Morreau,‡ and Hans Tanke*

From the Laboratory for Cytochemistry and Cytometry, Department of Molecular Cell Biology, the Department of Human Genetics,† and the Department of Pathology,‡ Leiden University Medical Center, Leiden, The Netherlands*

At present, limiting factors in the use of tissue microarrays (TMAs) for high-throughput analysis relate to the visual evaluation of the staining patterns of each of the individual cores in the array and to the subsequent input of the results into a database. Such a database is essential to correlate the data with tumor type and outcome, and to evaluate the performance against other markers achieved in separate experiments. So far, these steps are mostly performed by hand, and consequently are time-consuming and potentially prone to bias and errors, respectively. This paper describes the use of a high-resolution flat-bed scanner for digitization of TMAs with a resolution of about 5 × 5 μm^2. The arrays are acquired, the positions of the tissue cores are automatically determined, and measurement data including the images of the individual cores are archived. The program provides digital zooming of arrays for interactive verification of the results and rapid linkage of individual core images to data sets of other markers derived from the same array. Performance of the system was compared to manual classification for a representative set of arrays containing colorectal tumors stained with different markers. ***(J Mol Diagn 2003, 5:160–167)***

In 1998, Kononen et al[1] introduced tissue microarrays (TMAs) as a powerful technology to rapidly visualize molecular targets such as genes and gene products in thousands of tissue specimens at a time. TMAs are typically constructed by taking 0.6-mm cylindrical core specimens from morphologically representative regions in multiple paraffin blocks and positioning them one by one in a recipient paraffin block in which an array of holes has been drilled with slightly larger spacing (0.8 mm). The result is a new block that contains up to 1000 different tissues, all with detailed information about tumor type and grade as well as patient outcome, thereby greatly facilitating retrospective studies. The validity of TMA analysis in comparison to conventional tissue sampling has been shown, for instance, in cancers of the breast[2–3] and prostate.[4] The new block can be sectioned several hundred time depending on the length of the individual cores, implying that many different markers can be tested when needed in different laboratories on the same array; obviously noting that the properties of the individual tumors may change on repeated sectioning. TMAs are therefore ideally suited for rapid genomics-based evaluation of new diagnostic and prognostic molecular markers, ultimately leading to discovery and development of therapeutic targets.[5–17] TMAs may be stained using specific antibodies or nucleic acid probes, or labeled with enzymes or fluorophores as reporter molecules.

Compared to conventional visualization, the speed of molecular analysis is increased by a factor of more than a hundred. Construction of TMAs, originally done by hand, can be automated, increasing the throughput even more. At present, limiting factors in the use of TMAs for high-throughput analysis relate to the visual evaluation of the staining patterns of each of the individual cores in the array and to the subsequent input of the results into a database. Such a database is essential to correlate the data with tumor type and outcome, and to evaluate the performance against other markers, achieved in separate experiments. So far, these steps are mostly performed by hand, and are consequently time-consuming and potentially prone to bias and errors, respectively.

This problem has been recognized and, recently, attempts have been made to use automation and image analysis to address this issue.[18–19] Our approach in addressing these issues is to use digital scanning techniques and subsequent low-resolution image analysis to generate a classification code that is automatically stored in databases. The system is based on a flat-bed-type scanner ("top of the line color photocopier") that records images at zero optical magnification with a pixel resolution of about 5 × 5 μm^2. It provides digital zooming of arrays for interactive verification of the results and rapid linkage to data sets of other markers derived from the same array. Performance of the system was compared to manual classification for a representative set of arrays containing colorectal tumors stained with different markers.

Supported by the "Anna en Maurits de Kock Foundation."

Accepted for publication March 27, 2003.

Address reprint requests to Dr. Ir. J. Vrolijk, Department of Molecular Cell Biology, Leiden University Medical Center, Wassenaarseweg 72, 2333 AL Leiden, Netherlands. E-mail: j.vrolijk@lumc.nl.

Materials and Methods

Preparation and Staining of the Arrays

A TMA was constructed from formalin-fixed, paraffin-embedded tissues using 0.6-mm diameter punches obtained by a TMA puncher (Beecher instruments, Silver Spring, MD, USA). The array contained 362 tissue cores of colorectal tumors from 129 patients. Tumors selected were all from patients suspected of hereditary non-polyposis colorectal cancer (HNPCC). Suspicion of HNPCC was originally based on an early age of diagnosis, including distinct clinicopathological features (right-sided location and histology), or on a history of family members who also had a colorectal or extracolonic tumor diagnosed. The majority of tumors were tested for microsatellite instability (MSI) and immunohistochemical staining of *MLH1*, *MSH2*, or *MSH6*. One hundred four of one hundred twenty-nine tumors tested showed instability (primarily MSI-H). The TMA includes tumors from 45 known mutation carriers with mutation in *MLH1*, *MSH2*, or *MSH6*. The possible germ-line mutations were not detected or not yet determined from the remaining 84 patients. Included in the TMA were three tissue cores from normal colon mucosa (as control) and one core of lung tissue (for orientation). Using a tape-transfer system (Instrumedics, Hackensack, NJ, USA), 4-μm sections were transferred to coated glass slides. These TMA sections were subsequently analyzed for the immunohistochemical staining of *MLH1*, *MSH2*, and *MSH6* and compared with the results from previously stained whole sections of the tumors.[20] Staining for *MLH1*, *MSH2*, and *MSH6* was purposely chosen but was considered to result in staining intensities and patterns (tumor cells *versus* internal controls) that were too subtle to be reliably analyzed in the automated low-resolution image analysis system used here.

Furthermore, the arrays were analyzed for ki-67 (clone MIB1; DAKOCytomation, Glostrup, Denmark), P53 (clone DO-7; DAKOCytomation), β-catenin (clone 14; Transduction Labs, Lexington, KY, USA) and cytokeratin (Pan Ab-1, clone AE1/AE3; NeoMarkers, Fremont, CA, USA) staining. Cytokeratin analysis was included to automatically omit punches without cytokeratin positivity (epithelial fraction not present), thus preventing false-negative staining results.

P53 staining was manually classified according to the following four categories: category 1 when no cells showed nuclear staining (possibly mutated p53 or due to eg, mdm2 overexpression), category 2 for 0 to 25% staining (predicted wild-type p53), category 3 for 25 to 75% staining (possibly mutated p53), and category 4 for more than 75% of the cells showing strong nuclear staining (predictive for mutated p53). Ki67 staining was classified in a similar way. The four categories of β-catenin staining were distinguished as follows: category 1 when only membranous staining was seen, category 2 for nuclear staining on the peripheral edges of tumor, category 3 for elevated nuclear staining and membranous staining, and category 4 for strong nuclear expression and weak membranous staining.

Hardware Configuration

The system consists of a flat-bed Agfa XY-15 scanner interfaced to a 933MHz Power Mac G4 computer via a SCSI-2 interface. The computer is equipped with 512 MB memory and a 60 GB disk for image storage. The single pass XY-15 scanner can be used both in transparency and reflective mode, from which the former is applied for digitizing the microscopic slides. It has a tri-linear 8000 element charge coupled device (CCD) provided with optical XY-zoom technology. In this way an optical resolution of 5000 dots per inch (dpi) is obtained in both directions corresponding to about 5.0 μm. Sampling density can be increased further to 15000 dpi by means of interpolation. The maximum scan area is 350 $\times$ 455 mm, corresponding to A3+ format. However, the highest optical resolution is only achieved within the middle part of 232 $\times$ 455 mm. A special mold, which can accommodate 45 microscopic slides, has been constructed to fit on this part of the scanner. All slide holders are equipped with springs that press a slide against two notches, so that each slide position is well defined. The maximum density range of the scanner is 0 to 3.9, resulting in a color depth of 16 bit per Red Green Blue (RGB) color. Images of tissue microarrays and individual cores, including their derived features, can be archived on a large file server for reviewing the data via a local area network.

Image Acquisition

Stained sections were digitized using the ColorExact software package from Agfa, which additionally allows the setup of the scanner characteristics, such as scan mode, scan resolution, color calibration, and dynamic range. Usually a bed-scan of the complete scan area is performed first at a relatively coarse resolution of 100 dpi. Then the bed-scan is automatically analyzed for the presence of microscopic slides and for each slide the label and specimen part are determined. This provides the necessary information about the orientation of the tissue microarrays and the coordinates of the regions for scanning the arrays at a higher resolution. A batch job is thereby generated for the automatic scanning of these regions by ColorExact, so that up to 45 slides can be digitized automatically.

The tissue microarrays for this study were all sampled at about 5600 dpi just above the theoretical spatial resolution. Typical image sizes of 50 MB were obtained for tissue microarrays of 24 $\times$ 16 cores, while the images were scanned at a speed of about 30 MB per minute. Additional time is necessary to calibrate the scanner and to focus an image crop and takes 30 to 40 seconds. Autofocusing is based on an interpolation scheme, which is an integral part of the ColorExact software, and cannot be influenced by the operator. This focus procedure appeared to be sufficient for this study.

Image Analysis

The analysis of the TMAs was performed automatically and can be divided into the following steps: the determi-

nation of the grid size, the localization of the individual cores, the measurement of image features, and the evaluation and archiving of individual core data.

For segmenting the individual cores the color TMA image was converted to a gray-value image by equally averaging the separate RGB channels. On the basis of the gray-value histogram, an initial global threshold was determined to segment the individual cores from the background. The binary image was cleaned by removing small particles and partially detected cores utilizing morphology operations such as erosions and openings. The remaining objects were assumed to be tissue cores and features, such as size, center of gravity, and shape (eccentricity) were measured, while for each object the distances to its four nearest neighbors and the corresponding angles also were determined. The core size of the grid was calculated as an average from the objects, which were sufficiently round and was used later as an estimate for the detection of cores, which were not found initially or were incomplete.

A histogram based on the distances of the individual cores to their nearest neighbors was calculated to estimate the intercore spacing of the grid. The tissue microarrays analyzed in our laboratory showed little difference in spacing along the two main axes and did not result in significantly different peaks. The first peak in this histogram, in most cases also the highest peak, corresponds to distances belonging to 4-connective neighboring cores. For the distances, which lay within twice the SD of this peak, the angular histogram was also determined and corrected for eventual shifts of 180 degrees. The two highest peaks in this latter histogram, mostly at a distance of approximately 90 degrees from each other, correspond to the directions of the main axes. More accurate values of these directions were calculated by averaging only the angles, which lay within the SD of a peak value. Finally, the precise grid spacing in both directions separately was determined by averaging the distances belonging to the two peaks within the angular histogram separately.

This method for the determination of the grid characteristics requires that a sufficient number of cores are initially detected, so that mainly distances of those nearest neighbors are found, that are 4-connective. For the tissue microarrays, analyzed in our laboratory, this did not seem to present a problem.

The grid characteristics found in combination with the detected cores of the correct shape and size were used to fit an initial grid for the TMA. The positions of the remaining cores were determined by local bilinear interpolation and, when necessary, by predictive extrapolation. When the position of an interpolated core almost coincided with the position of an object that was initially detected but was not of the correct size and/or shape, the core position was adjusted to optimally cover the object area.

When cores are not exactly matched automatically, the operator still has the possibility to adapt the core positions interactively, so that the correct features are measured. In the TMA slides analyzed so far no real subarrays were present. Partially empty rows showed the same spacing as normal rows, so that no mismatches occurred as empty cores were fit in between. In principle, the program may be adapted so that also larger and more complex TMA slides may be handled.

Feature Extraction and Image Archiving

Since the resolution of the flat-bed scanner is not sufficient enough to analyze the individual cells within the tissue cores, only some global features were extracted to characterize each core. The cores were thereby segmented into parts containing probe signal and counterstain, while also empty or partially empty cores were found. In addition to area percentages, the total absorption of both the probe and counterstain parts were determined by summing the logarithmic intensity values corrected for the logarithmic value of the averaged background intensity of the corresponding pixels. Other parameters were also measured, such as peak intensity and parameters derived from the intensity histogram, to characterize the distribution of the intensities within the probe and counterstain class.

The numerical data were saved in an Excel spreadsheet to classify the different tissues and were organized as follows. A directory structure is created for each type of tissue array. The main directory contains a spreadsheet for each measured marker and a separate spreadsheet describing the organization and the content of the array. A subdirectory for each individual core is created where the corresponding images for the various markers reside. The measurements of the individual cores are organized row-wise in the spreadsheet, while a column is reserved for the file path to the corresponding image. Spreadsheets as generated by the pathologists containing the visual classification of the arrays in the traditional four classes can be easily combined with the spreadsheets of the measured data using a simple macro. In principle, an additional macro also can be written to reformat the data, so that it can be applied to hierarchical cluster analysis programs for tissue microarrays, as described recently by Liu et al.[18]

The analysis program itself can also retrieve both the measurement and image data for the different markers so that corresponding cores from different markers can be displayed simultaneously. This is considered very useful because it provides the pathologist with direct visual information as to how the expression of a set of markers differs for various cancer types.

Results

In Figure 1 the various steps of the image analysis procedure are shown to determine the grid and the position of the individual tissue cores on a microarray stained for p53. In all microarrays analyzed up to now, it appeared that after morphological filtering to reduce the noise particles (Figure 1b), enough tissue cores remained detectable to determine reliable estimates for the direction of the axes of the grid and for the spatial distance between neighboring cores. The interpolation algorithm for fitting the remaining cores, which were not round enough or

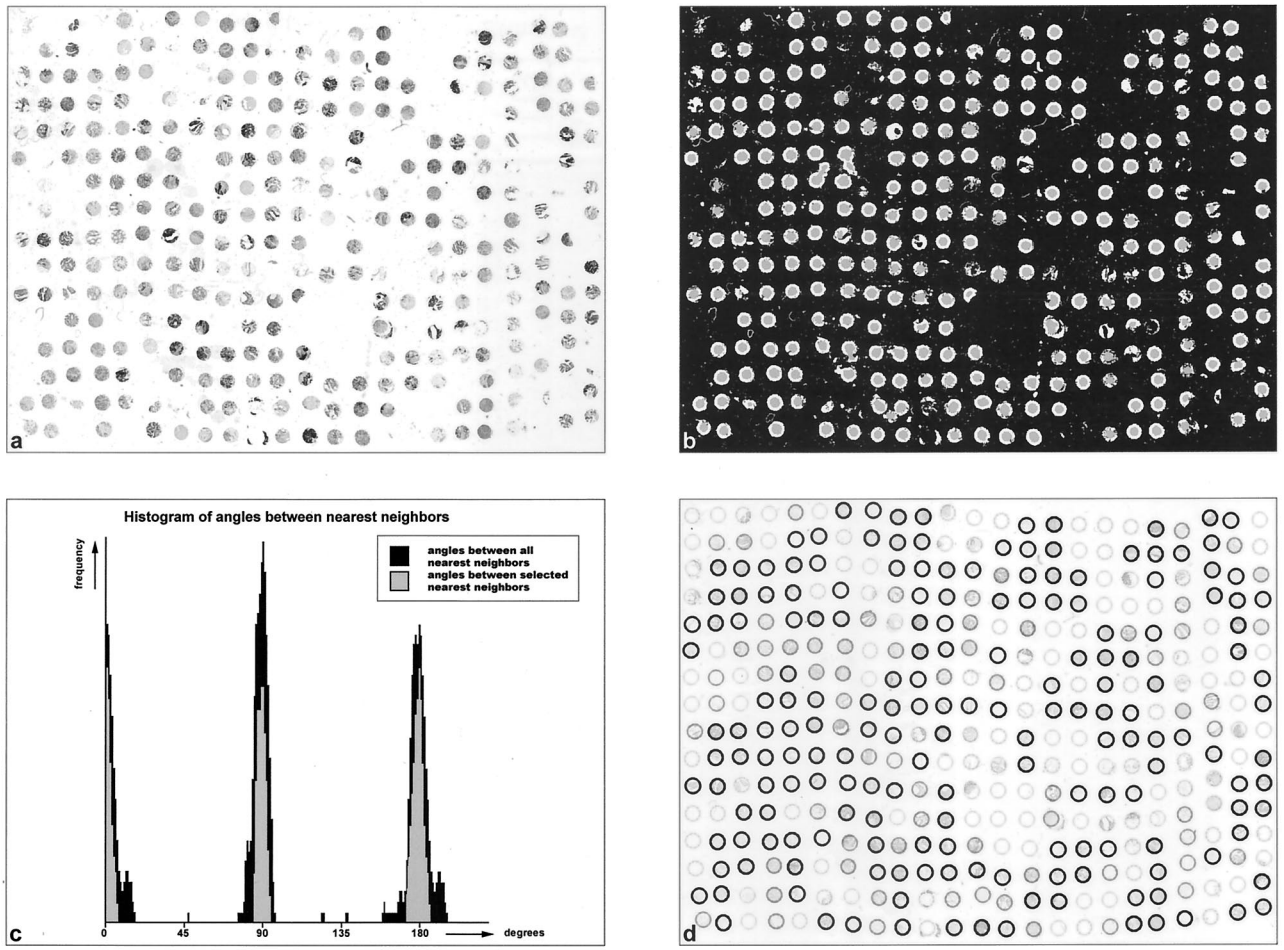

Figure 1. Determination of the grid of the tissue microarray. **a:** The gray-value image of a tissue microarray digitized at 5600 dpi. **b:** The thresholded image (**white + gray**) is morphologically filtered to select the tissue cores (**gray**). **c:** The histogram of the angles between all nearest neighbors (**dark gray**) and after selection of the neighbors for which the distance falls within the SD of the average distance (**light gray**). **d:** The tissue cores as found by the algorithm. **Black circles** indicate that the corresponding cores were used to estimate the grid characteristics, while **circles** are given in **gray** when a core is only partly detected; the **light gray circles** are solely based on interpolation.

were incomplete, also appeared to function satisfactorily. Only in rare cases, when a very small proportion (less than 10%) of a core was present and when it was lying considerably off-axis, human interaction seemed to be necessary to correct the automatically determined position.

A number of arrays of colorectal tumors stained for ki-67, p53, and β-catenin were analyzed to test the potentiality of the XY-15 flat-bed scanner for the analysis of TMAs. The arrays of 23 $\times$ 16 cores corresponding to 2.7 $\times$ 2 cm were digitized at 5600 dpi. The time necessary to scan those slides was about 2 minutes and 20 seconds per slide, 30 seconds of which were used for calibrating the lamp and focusing the image crop. The necessary amount of time to segment the individual tissue cores, measure the parameters, and add the core images to the database was 20 seconds per slide.

As the manual classification in four classes is based on the intensity of the probe signal and the proportion of the tissue that shows expression, the integrated absorption and the relative area of the probe signal were used to classify the tissue cores. In Figure 2, the results are shown for the nuclear markers, p53 and ki67, and the membrane marker β-catenin. The measurements on the nuclear markers show a good correlation with the visual classification in four classes by the pathologist, although the classes largely overlap. Correlation coefficients of 0.75 and 0.77 were measured for, respectively, the area and the integrated absorption of marker p53 and of 0.66 and 0.72 for ki67. Such a correlation is not present for the membrane marker β-catenin, as correlation coefficients of 0.10 and 0.21, respectively, were obtained. In Figure 2d, the absorption distribution is shown as a function of the total absorption for p53 expression. The absorption distribution is a parameter derived from the absorption histogram by non-linear weighting of the various absorption classes. However, this parameter or other parameters which were measured, such as peak intensity, average intensity of the marker, and relative marker area, did not significantly improve the classification results.

The program to analyze the TMAs has the ability to retrieve corresponding cores from different TMAs to visualize the expression of different markers on a certain cancer. Although the resolution (about 5 $\times$ 5 μm per pixel) is not high enough to recognize single-stained

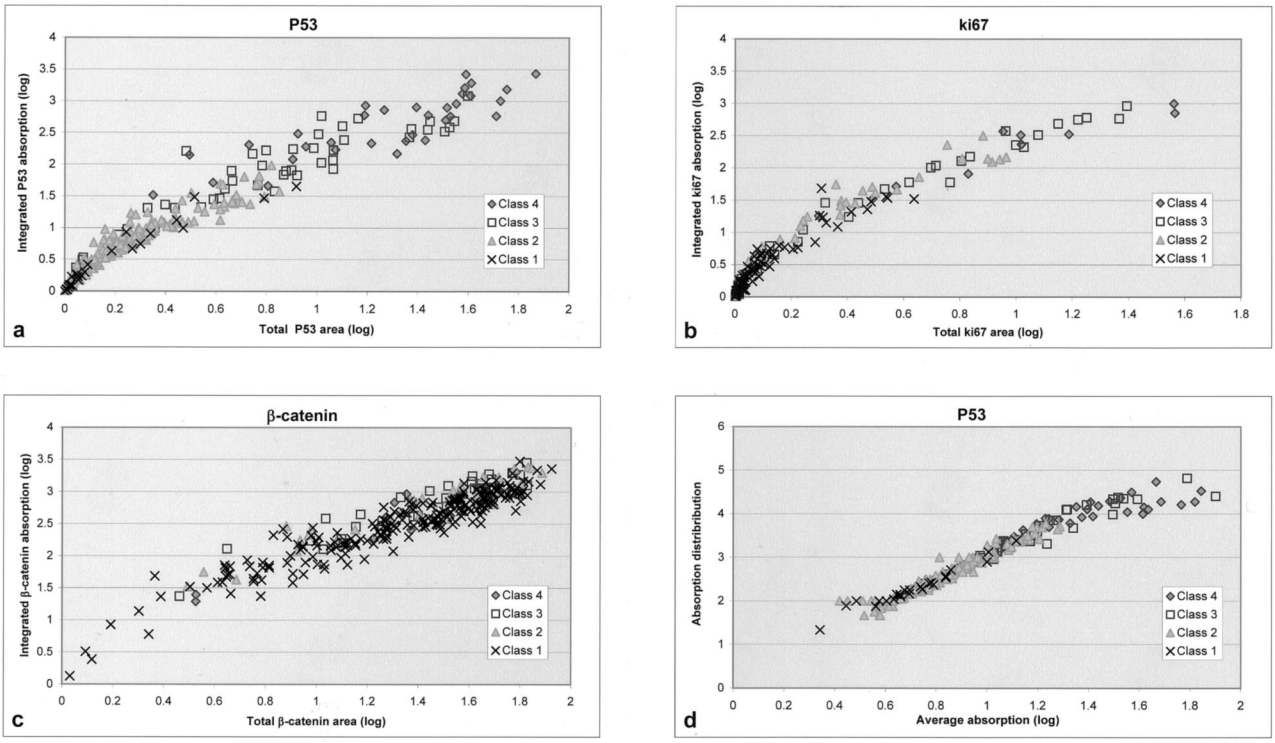

Figure 2. The measured absorption values of tissue cores of colorectal tumors, visually classified in four classes, are shown as function of the measured probe area for p53, ki67, and β-catenin, respectively. Additionally the absorption distribution is shown as a function of the total absorption for the p53 expression marker.

cells, it provides a good impression of the tissue structure and the amount of probe single present. This was particularly true for parameters such as ki67 and p53, which typically imply nuclear staining of varying intensity. Membrane-bound markers such as β-catenin with a much more patch-like pattern lost their original appearance due to a lack of spatial resolution. In Figure 3, corresponding cores of tissue microarray stained with p53, ki67, and β-catenin are shown illustrating the resolution that can be achieved by flat-bed scanning. In Figure 4, part of a tissue core stained for p53 is electronically zoomed out to the cellular level and compared to the corresponding microscopic image digitized using a 10× objective. This clearly illustrates the limited resolution of the flat-bed scanner. Cells appear as out-of-focus blobs and cannot be individually recognized.

Discussion

This paper describes a method for the automatic acquisition of tissue microarrays. Grid characteristics, such as size, amount of rotation, orientation, and intercore distance are determined automatically and consecutively in addition to the locations and the array indices of the individual cores. Subsequently, the corresponding images are stored for archiving. The method appears to be robust and relatively insensitive to rotations of the grid and can cope with a number of cores being absent or incomplete.

Despite the rather low resolution of the flat-bed some global measurements are performed to classify the individual cores. The results of this pilot study are encouraging. Especially for nuclear markers, such as p53 and ki67, requiring relatively low spatial resolution, classification based on the integrated absorption and the probe area show a similar trend when compared to the visual classification by the pathologist, although the classes still show a large overlap. For membrane markers, such as β-catenin, which requires higher spatial resolution, the resolution of the flat-bed scanner appears to be too low to provide similar results. Some improvements were obtained by combining the measurements of the markers with the presence of sufficient amount of cytokeratin positivity in the TMA of a neighboring cross-section. This eliminates cores for which the integrated absorption is based on a relatively small proportion of the cancerous tissue. A recent and more extensive study by Camp et al[19] has shown that automatic analysis of tissue microarrays has a better reproducibility than visual pathologist-based scoring, although the continuous scale of automated classification tends to overlap with the visual-based scoring in four discrete classes. However, it shows that for β-catenin expression in TMAs of colon cancer, automated analysis of subcellular compartments is able to discern subtle differences in staining intensity resulting in new subsets of tumors with prognostic significance, which is not seen using visual pathologist-based assessment.

A separate study to evaluate the visual classification of TMAs by comparing the staining of whole tumor slides *versus* the results on TMAs showed that in the case of p53 and ki67 the four different classes could be reliably recognized in TMAs. However, the visual classification for

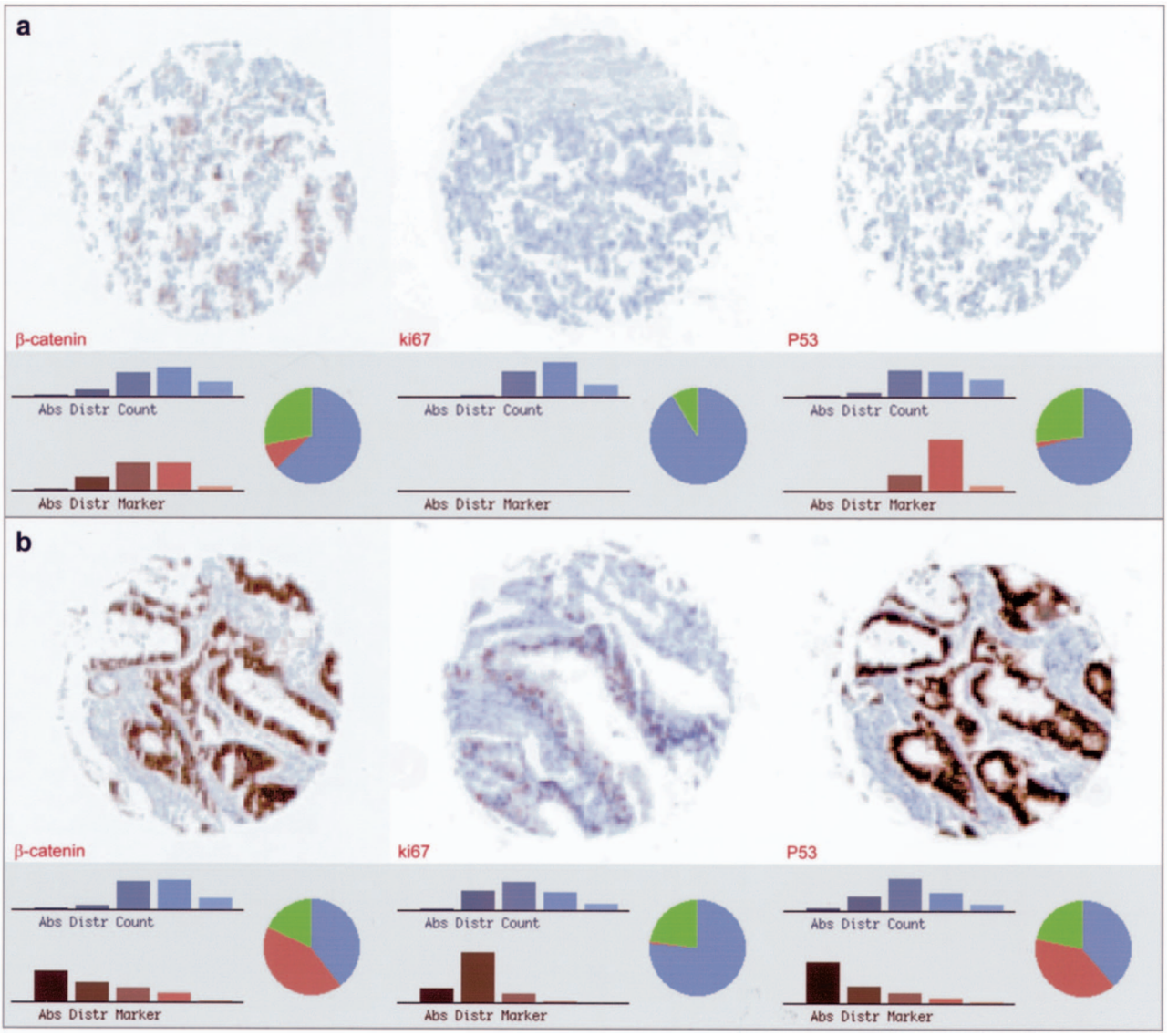

Figure 3. A number of corresponding tissue cores of different TMAs are shown for the expression markers β-catenin, ki67, and p53. The resolution is about 5 × 5 um per pixel. The manual classification was class 1 for all markers of case **a**. For case **b** the β-catenin expression was found to be of class 3, the ki67 expression class 2, and the p53 expression class 4.

β-catenin-stained TMAs appeared also to be much more difficult; since only category 4 corresponding to a strong nuclear expression and weak membranous staining could be reliably confirmed in whole tumor slides, while the three other categories could not easily be distinguished in the TMAs as separate staining patterns.

Currently the tissue cores are segmented into areas containing the expression marker, the counterstain, and eventually in areas with no cellular material present and absorption measurements are performed on these different parts. It was hypothesized that a better method might be to calculate the absorption through calibrating the exact colors of the counterstain and the expression marker using reference cores, and then integrate the contributions per pixel to the different classes. However, this method did not result in a significantly better classification. We also tested whether over-sampling above the optical resolution to 15000 dpi would improve the results. Indeed, the over-sampled images of the individual tissue cores looked better on the screen, when compared to those digitized at the optical resolution and re-sampled at the same interpolated resolution using the bi-cubic interpolation scheme of Photoshop. However, the classification results of the TMAs showed no improvement. Over-sampling has almost no influence on the acquisition time and increases the analysis time only marginally. However, the database will grow by a factor of 6 due to the increased image size of the cores.

The analysis program is capable of automatically processing the TMAs without any human interaction. Only tissue cores, which are incomplete, are sometimes not optimally covered by the bilinear interpolation and predictive extrapolation algorithm. An algorithm, to optimize the fitting between cores, as found by interpolation and the amount of tissue present in the direct vicinity, could probably improve this further, so that no human interac-

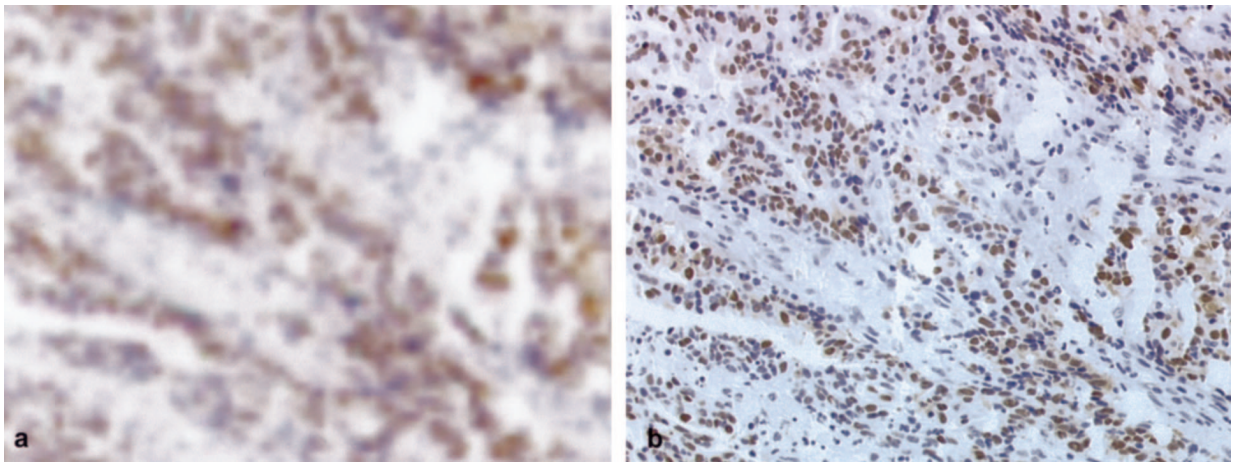

Figure 4. Comparison between the image quality of the AGFA XY-15 flat-bed scanner and the microscope using a 10× objective. **a:** Part of a tissue core stained for P53 digitized on the flat-bed scanner and electronically zoomed out to the cellular level. **b:** The corresponding microscopic image digitized using a 10× objective.

tion would be necessary even when the initial fit is not optimal.

It appeared to be very useful to combine the analysis of TMA slides with hands-off data input in a database for visualization of the tissue cores. It provides the pathologist with direct visual feedback on how the expression signals can differ for different types of cancer and it shows also how the expression patterns may vary for patients with the same type of tumor. Furthermore, it avoids errors related to the manual input of data that are considered substantial. Realizing that the use of TMA easily leads to input of thousands of data points, automated classification and data input seem to be the only solution.

The resolution of the Agfa scanner appeared to be sufficient for the analysis of the nuclear markers, while it was still too low to classify the tissues stained with membrane markers and to identify the individual cells visually. This would require at least a resolution improvement of a factor of 3 to 4. However, it is unlikely that the resolution of flat-bed scanners will improve in the near future. The optical resolution of the Agfa XY-15 is already among the highest currently available and is below the grain size as used in photographic films, so that the need for higher resolution is hardly present for the graphic industry, where most of these systems are sold.

On the other hand, a similar approach for the processing of TMAs could also be followed using a microscope system with an automated scanning stage, objective revolver, autofocus, CCD camera, and, optionally, a slide feeder, when large numbers of TMAs have to be analyzed. A TMA could first be scanned at a relative low magnification (using a 2.5 to 10× objective) to determine the grid characteristics and the positions where the individual cores are located. The individual tissue cores could then be acquired at a higher magnification (using a 20 to 40× objective) by stitching separate CCD images together when necessary. At present, commercial systems including automated slide loading are available. The algorithms for automated processing of TMA slides at low magnification as described in this paper and image acquisition of individual cores at high magnification can easily be implemented in such systems. The program in its current form is, however, available for the scientific community.

The automated microscopic approach for analyzing tissue microarrays will result in much larger images for the tissue cores (about 1 to 5 MB at 0.5-μm resolution), but with the ongoing development of faster PCs and steadily increasing data storage facilities it is feasible to easily store millions of tissue sections into a database. This provides the pathologist not only with the ability to directly retrieve and visualize the expression patterns for various cancers, but also with the possibility to zoom into the cellular level.

Acknowledgments

We thank Dr. Joe Gray of the San Francisco Cancer Center for help and advice.

References

1. Kononen J, Bubendorf L, Kallioniemi A, Barlund M, Schraml P, Leighton S, Torhorst J, Mihatsch MJ, Sauter G, Kallioniemi OP: Tissue microarrays for high-throughput molecular profiling of tumor specimens. Nat Med 1998, 4:844–847
2. Gillett CE, Springall RJ, Barnes DM, Hanby AM: Multiple tissue core arrays in histopathology research: a validation study. J Pathol 2000, 192:549–553
3. Camp RL, Charette LA, Rimm DL: Validation of tissue microarray technology in breast carcinoma. Lab Invest 2000, 80:1943–1949
4. Mucci NR, Akdas G, Manely S, Rubin MA: Neuroendocrine expression in metastatic prostate cancer: evaluation of high-throughput tissue microarrays to detect heterogeneous protein expression. Hum Pathol 2000, 31:406–414
5. Barlund M, Forozan F, Kononen J, Bubendorf L, Chen Y, Bittner ML, Torhorst J, Haas P, Bucher C, Sauter G, Kallioniemi OP, Kallioniemi A: Detecting activation of ribosomal protein S6 kinase by complementary DNA and tissue microarray analysis. J Natl Cancer Inst 2000, 92:1252–1259
6. Barlund M, Monni O, Kononen J, Cornelison R, Torhorst J, Sauter G, Kallioniemi OP, Kallioniemi A: Multiple genes at 17q23 undergo am-

plification and overexpression in breast cancer. Cancer Res 2000, 60:5340–5344
7. Bowen C, Bubendorf L, Voeller HJ, Slack R, Willi N, Sauter G, Gasser TC, Koivisto P, Lack EE, Kononen J, Kallioniemi OP, Gelmann EP: Loss of NKX3.1 expression in human prostate cancers correlates with tumor progression. Cancer Res 2000, 60:6111–6115
8. Bubendorf L, Kononen J, Koivisto P, Schraml P, Moch H, Gasser TC, Willi N, Mihatsch MJ, Sauter G, Kallioniemi OP: Survey of gene amplifications during prostate cancer progression by high-throughout fluorescence in situ hybridization on tissue microarrays. Cancer Res 1999, 59:803–806
9. Bubendorf L, Kolmer M, Kononen J, Koivisto P, Mousses S, Chen Y, Mahlamaki E, Schraml P, Moch H, Willi N, Elkahloun AG, Pretlow TG, Gasser TC, Mihatsch MJ, Sauter G, Kallioniemi OP: Hormone therapy failure in human prostate cancer: analysis by complementary DNA and tissue microarrays. J Natl Cancer Inst 1999, 91:1758–1764
10. Hedenfalk I, Duggan D, Chen Y, Radmacher M, Bittner M, Simon R, Meltzer P, Gusterson B, Esteller M, Raffeld M, Yakhini Z, Ben-Dor A, Dougherty E, Kononen J, Bubendorf L, Fehrle W, Pittaluga S, Gruvberger S, Loman N, Johannsson O, Olsson H, Wilfond B, Sauter G, Kallioniemi OP, Borg A, Trent J: Gene expression profiles of hereditary breast cancer. N Engl J Med 2001, 344:539–548
11. Miettinen HE, Jarvinen TA, Kellner U, Kauraniemi P, Parwaresch R, Rantala I, Kalimo H, Paljarvi L, Isola J, Haapasalo H: High topoisomerase II α expression associates with high proliferation rate and poor prognosis in oligo-dendrogliomas. Neuropathol Appl Neurobiol 2000, 26:504–512
12. Moch H, Schraml P, Bubendorf L, Mirlacher M, Kononen J, Gasser T, Mihatsch MJ, Kallioniemi OP, Sauter G: High-throughput tissue microarray analysis to evaluate genes uncovered by cDNA microarray screening in renal cell carcinoma. Am J Pathol 1999, 154:981–986
13. Perrone EE, Theoharis C, Mucci NR, Hayasaka S, Taylor JM, Cooney KA, Rubin MA: Tissue microarray assessment of prostate cancer tumor proliferation in African-American and white men. J Natl Cancer Inst 2000, 92:937–933
14. Richter J, Wagner U, Kononen J, Fijan A, Bruderer J, Schmid U, Ackermann D, Maurer R, Alund G, Knonagel H: High-throughput tissue microarray analysis of cyclin E gene amplification and overexpression in urinary bladder cancer. Am J Pathol 2000, 157:787–794
15. Schraml P, Kononen J, Bubendorf L, Moch H, Bissig H, Nocito A, Mihatsch MJ, Kallioniemi OP, Sauter G: Tissue microarrays for gene amplification surveys in many different tumor types. Clin Cancer Res 1999, 5:1966–1975
16. Tynninen O, Paetau A, von Boguslawski K, Jääskeläinen J, Aronen HJ, Paavonen T: p53 expression in tissue microarray of primary and recurrent gliomas. Brain Pathol 2000, 10:575–576
17. Kallioniemi OP, Wagner U, Kononen J, Sauter G: Tissue microarray technology for high-throughput molecular profiling of cancer. Hum Mol Genet 2001, 10:657–662
18. Liu CL, Prapong W, Natkunam Y, Alizadeh A, Montgomery K, Gilks CB, van de Rijn M: Software tools for high-throughput analysis and archiving of immunohistochemistry staining data obtained with tissue microarrays. Am J Pathol 2002, 161:1557–1565
19. Camp RL, Chung GG, Rimm DL: Automated subcellular localization and quantification of protein expression in tissue microarrays. Nat Med 2002, 11:1323–1327
20. Hendriks Y, Franken P, Dierssen JW, de Leeuw W, Wynen J, Dreef E, Tops C, Breuning M, Bröcker-Vriends A, Vasen H, Fodde R, Morreau H: Conventional and tissue microarray immunohistochemical expression analysis of mismatch repair in hereditary colorectal tumors. Am J Pathol 2003, 162:460–477